Process optimization of reservoir fines trapping by mesoporous silica nanoparticles using Box-Behnken design

Augustine Agi [a,b], **Radzuan Junin** [a,b,*], **Mohd Zaidi Jaafar** [a,b,*],
Nor Aishah Saidina Amin [c], **Mohd Akhmal Sidek** [a,b], **Faruk Yakasai** [a,e],
Azrul Nurfaiz Mohd Faizal [d,f], **Afeez Gbadamosi** [g], **Jeffrey Oseh** [h]

[a] *Department of Petroleum Engineering, School of Chemical and Energy Engineering, Faculty of Engineering, Universiti Teknologi Malaysia, 81310 Johor Bahru, Malaysia*
[b] *Institute for Oil and Gas (IFOG), Universiti Teknologi Malaysia, 81310 Johor Bahru, Malaysia*
[c] *Chemical Reaction Engineering Group (CREG), School of Chemical and Energy Engineering, Faculty of Engineering, Universiti Teknologi Malaysia, 81310 Johor Bahru, Johor, Malaysia*
[d] *Department of Chemical and Energy, School of Chemical and Energy Engineering, Faculty of Engineering, Universiti Teknologi Malaysia, 81310 Johor Bahru, Johor, Malaysia*
[e] *Department of Chemical and Petroleum Engineering, Faculty of Engineering, Bayero University, Kano PMB 3011, Nigeria*
[f] *Centre of Lipids Engineering & Applied Research (CLEAR), Ibnu-Sina Institute for Scientific & Industrial Research (ISI-SIR), Universiti Teknologi Malaysia, 81310 UTM Johor Bahru, Johor, Malaysia*
[g] *Department of Chemical and Petroleum Engineering, College of Engineering, Afe Babalola University, PMB 5454 Ado-Ekiti, Ekiti State, Nigeria*
[h] *Department of Petroleum Engineering, School of Engineering and Engineering Technology, Federal University of Technology, P.M.B. 1526 Owerri, Imo State, Nigeria*

Abstract Mesoporous silica nanoparticles (MSNP) were used to trap reservoir fines and adsorption capacity of MSNP was optimized. Box-Behnken design was used to model effect of concentration, time, salinity and pH on adsorption capacity of reservoir fines. Multiple response surface method was applied to optimize any combination of variables at which the maximum adsorption of the reservoir fines occurred. Microstructural analysis shows a mesoporous structure ranging from 2.88 to 44.8 nm with high specific surface area of 332 m^2/g and purity of 94%. Pseudo-second order with regression coefficient (R^2) of 0.99 shows that the model best defines reservoir fines adsorption. Langmuir isotherm model with R^2 of 0.985 best fitted the equilibrium adsorption of kaolinite whereas high R^2 of 0.98 and lower sum of squared errors of illite for Freundlich model indicates it is better than Langmuir model. Heterogeneity factor value of $1/n < 1$ and n values of 5–11 shows

* Corresponding authors at: Department of Petroleum Engineering, School of Chemical and Energy Engineering, Faculty of Engineering, Universiti Teknologi Malaysia, 81310 Johor Bahru, Malaysia (M. Zaidi Jaafar).
E-mail addresses: r-radzuan@utm.my (R. Junin), mzaidi@utm.my (M. Zaidi Jaafar).
Peer review under responsibility of Faculty of Engineering, Alexandria University.

sufficient site for adsorption. Predicted reservoir fines adsorption with R^2 of kaolinite (98.77%) and illite (99.32%) close to unity indicates that the model is highly consistent with the experimental results with high precision and reliability. Experimental and statistical analysis proved that MSNP can fixate reservoir fines and has adequate capacity to be rejuvenated and reused.

1. Introduction

The increased global demand for fossil fuel has necessitate oil and gas companies to venture into unconventional deep off-shore reservoirs [1–3]. This is because deep oil and gas reservoirs have good formations with high porosity and permeability. However, due to the harsh reservoir condition (high temperature and pressure), deep reservoirs are unconsolidated. Consequently, unconsolidated cementation is likely to result in fines migration. Fines migration in reservoir can significantly decrease permeability, which can affect the oilwell production, injection performance and subsequently formation damage [4]. Reservoir fines are materials that are cemented onto the skeleton of rock particles or are loose/unconsolidated particles in pore spaces. Reservoir fines are typically < 37 µm in diameter and consist of clay minerals such as kaolinite and illite [4,5]. Due to the physical, chemical and hydrodynamic effect of working fluids, incompatibility with fluid salinity, wettability of porous media, temperature, fractional flow of oil or water, pH, fluid flow rate and the presence of oil, these fines dislodge from the surface of pores and migrate blocking pore throats thereby, causing formation damage [6,7].

Conventional methods such as acidizing, hydraulic fracture, clay stabilizers are used to treat damaged formation caused by fines migration. But these conventional methods have some disadvantages such as well corrosion, plenty of surface equipment are required, operational problem of proppant, reduced efficiency during repetition of treatment, operating cost, safety and environmental concerns. These methods have limited their focus on tackling fines migration to near wellbore formation instead of eliminating the cause of the damage. The right solution is looking beyond the wellbore into the reservoir where the fines are generated [8]. Several researchers have proposed the use of chemical injection such as cationic and water-soluble polymers to flocculate or agglomerate the fines. However, these techniques were not effective because of polymers degradation at high temperature and pressure, high cost of polymers and large amount of polymers were required for effective treatment [7].

Previous studies have reported the use of nanoparticles to control fines migration [4,6,7,9–11]. Nanoparticles have high surface area which enables them to fixate mobile fines by adsorbing onto the fines thereby, decreasing repulsive force amongst reservoir fine and rock grain. Consequently, retaining the fines and prevent them from further migration. Therefore, the superlative approach to avert fines movement is to retain them at their original site or source [6]. This can be achieved either by rate reduction or settling of the reservoir fines. For instance, Mansouri et al. [9] investigated the effect of silica (SiO_2), aluminium oxide (Al_2O_3) and magnesium oxide (MgO) nanoparticles in controlling fines migration caused by low salinity injection in the presence of hydrocarbon. They reported that SiO_2 nanoparticles had a great potential to control fines migration during low salinity flooding compared to Al_2O_3 and MgO. Likewise, Shafian et al. [12] explored the use of colloidal SiO_2 nanoparticles (C-SNPs) to control fines migration. Core flooding experiments were performed to ascertain efficacy of C-SNPs in controlling fines migration at various temperature. C-SNPs modified the pore walls by attaching on the wall hence, migration of the fines was not noticed even at high injection rate. In similitude, Mansour et al. [11] investigated the effect of flow rate on fines displacement from grain surface. This was done by altering surface potential amongst the fines and grain surface. The results indicate that SiO_2 and MgO nanoparticles can adsorb on pore surface thereby, reducing repulsive force amongst the reservoir fines and pore surface. Monfared et al. [13] described the mechanisms of nanoparticles adsorption process onto reservoir fines during flooding. The first step is the film diffusion of the reservoir fines from bulk to the surface. Secondly, interparticle diffusion of reservoir fines to adsorption site occurs. Lastly, the reservoir fine is adsorbed at a site on the surface (internal/external) of the nanoparticle. Whereby, the rate of adsorption is usually controlled by film or interparticle diffusion or both rather than the latter, which is a slow process.

Industrial growth has led to increase in waste generation; a large amount of waste is currently being generated from palm oil industry. About 70% of the waste generated during palm oil extraction process are from discarded fresh empty fruit bunch (EFB) while the remaining 30% is from palm kernel shell, mesocarp fibre and palm mill effluent [14]. Disposal of these waste has become a major problem and ineffective treatment may cause serious environmental challenges. Nevertheless, these wastes can be used as starting raw material to produce new advanced materials such as SiO_2 nanoparticles owing to their environmental friendliness, availability, reusability, large surface area. Chemical treatment has been used to produce SiO_2 nanoparticles from renewable sources to enhance their adsorption capacity and ion exchange. However, this process requires chemicals that are not environmentally friendly, the process can be expensive, and the presence of contaminants affects the productivity of SiO_2 nanoparticles [15,16]. Therefore, the synthesis method and the removal of impurities before reaction is one of the obstacles faced in the production of SiO_2 nanoparticles [16,17]. These problems can be circumvented by intensification of synthesis and treatment methods.

Wet milling is a physical synthesis method used to design material for a specific application. These can be achieved by assigning the product with a specific surface area and porosity during the milling process. The advantage of this method is that it can minimize waste by producing nanoparticles that are easy to handle and can improve properties of the nanoparticle for better flowability [18]. However, poor wetting during

milling causes component segregation and broad particle size distribution [18]. Ultrasonication treatment is a process intensification method used for redispersion, facilitating mixing, chemical reaction, surface interaction, heat and mass transfer to produce particles with small size range [1,2,19].

Furthermore, conventional methods of experimental optimization require large numbers of runs which is time consuming and requires more chemicals [20]. Also, conventional methods are unable to offer interactional data between certain variables [21]. Nevertheless, experimental designs like response surface methodology (RSM) can be used to circumvent these limitations by evaluating the impacts of the various variables simultaneously and predict the optimum condition for the desirable response [22,23].

Previous studies have focused on injection rate reduction in mitigating against fines migration [9,11,12]. The use of ultrasound-assisted wet milling to synthesize mesoporous SiO_2 nanoparticles (MSNP) to trap reservoir fines at static condition is novel. Also, the optimization of the reservoir fines adsorption capacity using MSNP has not been reported in literature. Therefore, the main objective of this study is to produce environmentally friendly MSNP from EFB waste through wet milling and ultrasonication and to investigate the potential of the MSNP in trapping reservoir fines at static condition. Besides, the MSNP can also find usefulness in enhanced oil recovery, drilling fluid and environmental remediation. Herein, adsorption kinetic and isotherms models were utilized to conceptualize the adsorption procedures. Box-Behnken design (BBD) was used to model the effect of concentration, time, salinity and pH on the adsorption capacity of the reservoir fines by MSNP. Different parameters of the model were evaluated using statistical analysis of variance (ANOVA). Finally, a multiple RSM was applied to optimize any combination of the variables at which the maximum adsorption of the reservoir fines occurred. It is hypothesized that with this study environmental challenges associated with waste disposal, the use of expensive chemical to remove impurities before reaction, poor wetting during milling, fines migration in oilfield reservoir and the interaction between certain variables to predict the optimum response can be circumvented.

2. Materials and methods

2.1. Materials

EFB waste was obtained from Felda Palm Oil Mill, Kulai, Johor, Malaysia. Ethanol (biological grade) with a molecular weight of 46.07 g/mol and purity of 99.8% (v/v) was supplied by R & M Chemicals, Selangor, Malaysia. Sodium hydroxide (NaOH), hydrochloric acid (HCl, 37%) and natural kaolinite (molecular weight of 258.16 g/mol) were purchased from Sigma-Aldrich Chemie GmbH, Taufkirchen, Germany. Natural illite was obtained from Kuala Rompin, Pahang, Malaysia. Sodium chloride (NaCl) with molecular weight of 58.44 g/mol and purity of 99.8% was supplied by QReC^{TM}, Selangor, Malaysia.

2.2. Methods

2.2.1. Thermal treatment

EFB was washed with distilled water to remove dirt and sun dried to reduce the moisture thereafter, it was incinerated to obtain ash. The dried empty fruit bunch ash (EFBA) was thermally treated at 1100 °C using chamber furnace (Carbolite Gero 300) for 4 h and left to cool inside the furnace. This temperature range was chosen because crystallization of SiO_2 occurs above 800 °C [19] and above 1100 °C no significant change occurred.

2.2.2. Synthesis of MSNP

About 40 g of the treated EFBA was placed in a holder made of tungsten carbide, then it was packed with 150 mL of milling balls of the same material. The grinding jar (holder) was placed eccentrically in a Retsch PM 100 planetary ball mill equipment (Figure S1a, supplementary data). In this way, the rotation of the sun wheel with respect to the grinding bowl was the ratio of 1:2. Dry milling of EFBA was initiated for 20 min (rotating-reverse motion) at 10-minutes intervals for 2 h. Subsequently, 10 mL of ethanol was added to the EFBA and this time the ball speed (500 rpm) and the grinding jar created an interaction (frictional forces) releasing high energy to the EFBA for 4 h (Figure S1b). Consequently, the exchange of these forces resulted in comminution. The sample was then washed with ethanol and placed in an ultrasonic bath (Genesis^{TM} XG-500–6, 40 kHz, 500 W) for 1 h. The sample was then centrifuged and dried in an oven for 24 h.

2.2.3. Characterization of MSNP and reservoir fines

The elemental composition of EFBA was analysed by energy dispersion X-ray fluorescence (XRF) (EDXRF, Rigaku NEX CG Japan). It was operated under helium at 0.6 L/min and the weight percentages in the form of oxides were determined. The shape and size of the EFBA was studied using Hitachi S-3400 N scanning electron microscope (SEM) with a back-scattering electron detection. A high-resolution transmission electron microscopy (TEM) (HRTEM, JEOL, JEM-ARM200F) was used to determine size and shape of the MSNP. Detection was achieved at an accelerating voltage of 200 kV. A Gatan microscopy suite (GMS3) software was used to analyse the TEM image and the particles sizes determined. The morphology of the reservoir fines and adsorption process were visualized by field emission scanning electron microscopy (FESEM) (SU8020 HITACHI, Tokyo, Japan). The samples were coated using an automated platinum sputter coater (Quorum, Q150 RS, UK). The textural properties of MSNP were determined by nitrogen adsorption–desorption isotherms measured at 77.3 K on a Thermo Scientific Surfer Instrument. The samples were degassed in vacuum at 80 °C for 24 h. Thereafter, the specific surface area was calculated using Brunauer-Emmett-Teller (BET) method. Barrett-Joyner-Halenda (BJH) and Horvath and Kawazoe (HK) models were used to determine the mesopore and micropore size distribution from the desorption isotherm, respectively. Consequently, the relative pore volume was estimated from the adsorbed amount at relative pressure (p/p_0) between 0.31 and 1 and 0–0.35, respectively. The functional groups of MSNP before and after adsorption was detected by Fourier transform infrared spectroscopy (FTIR) (Frontier, PerkinElmer). The samples were mixed with potassium bromide and compressed under high pressure to form a pellet. The pellet was used for FTIR measurement at room temperature in the range of 650–4000 cm^{-1}. X-ray diffraction spectroscopy (XRD) (Rigaku SmartLab, Japan) analysis was used to determine

the composition of MSNP and reservoir fines. The device was operated at 40 kV, 30 mA with a Cu K-beta irradiation. The scanning angle of diffraction (2θ) ranged from 3 to 100° at a scanning speed of 8.2551 deg/min.

2.2.4. Batch adsorption studies

About 0.05 g of MSNP was added to 50 mL of reservoir fines solution at various concentration (5–25 mg/L). The concentration was determined at various time interval using a UV–vis spectrophotometer (Spectrum Lab 752 Pro) via 394 nm for illite and 400 nm wavelength for kaolinite. The adsorption capacity was determined using Equation (1).

$$q_t = \frac{(C_O - C_t)V}{m} \tag{1}$$

whereas q_t is adsorption of reservoir fines by MSNP (mg/g), C_o is initial concentration of reservoir fines (mg/L), C_t is concentration of reservoir fines (mg/L) at time t, V is volume of reservoir fines solution (L) and m is mass of MSNP added (g). Kinetic data was studied by means of pseudo-first and pseudo-second order models Equations (2) and (3), respectively.

$$q_t = q_e\left(1 - e^{-K_1 t}\right) \tag{2}$$

$$q_t = \frac{K_2 q_e^2 t}{1 + K_2 q_e t} \tag{3}$$

whereas q_e is the adsorbed adsorbate per unit mass of adsorbent (mg/g), K_1 (h^{-1}) and K_2 (g/mg h) are pseudo-first and second order constants. For the effect of concentration 0.05 g of MSNP was added to 50 mL of reservoir fines of various concentration (50–1000 mg/L). Thereafter, the solutions were left for five days (120 h) at ambient temperature to achieve equilibrium and the residual concentration was determined. The capacity at equilibrium was calculated by mass balance.

$$q_e = \frac{C_o - C_e}{m}V \tag{4}$$

whereas q_e is adsorption capacity at equilibrium (mg/g) and C_e is equilibrium concentration. The isotherm data were analysed and fitted to Langmuir (Equation (5)) and Freundlich (Equation (6)) models. The models were determined via non-linear regression method using Solver in MS Excel. This was done through reducing the sum of squared errors (SSE) to generate the best coefficient of determination (R^2).

$$q_e = \frac{q_m K_L C_e}{1 + K_L C_e} \tag{5}$$

$$q_e = K_F \tag{6}$$

whereas q_m is maximum adsorption capacity (mg/g), K_L is Langmuir constant (L/mg), K_F is Freundlich constant (mg/g) $(L/mg)^{1/n}$ and $1/n$ is dimensionless heterogeneity factor. To determine the effect of salinity 0.05 g of MSNP was dispersed in different concentrations (0.5 – 2.2 wt%) of NaCl. The range of salinity was selected based on literature [19]. Thereafter, 50 mL of reservoir fines at a fixed concentration of 50 mg/L was added to the solutions. The solution was left for five days to achieve equilibrium and the residual concentration was determined. To investigate the effect of pH on the adsorption of reservoir fines by MSNP, 0.05 g of MSNP was dispersed in

solution with preadjusted pH range of 2–10. The solution pH was adjusted using 0.5 M NaOH or 0.5 M HCl. Then, 50 mL of reservoir fines at a fixed concentration of 50 mg/L was added to the solutions. The solutions were kept for five days to achieve equilibrium and the concentration determined.

2.2.5. Desorption and reusability study

For the desorption study, 1 g/L of MSNP was added to 100 mL solution containing 10 mg/L of reservoir fines and stirred for 60 min. After each adsorption cycle, the MSNP was removed from the solution and washed thoroughly with distilled water to remove excess reservoir fines precipitated on the MSNP surface. Thereafter, the MSNP was dispersed in 50 mL solution containing 0.5 M of NaOH and stirred for 120 min. The reservoir fines concentration in the filtrate was determined using UV–vis spectrophotometer. The adsorption–desorption experiment was performed in eight cycles and the reusability of the MSNP was determined.

2.2.6. Design of experiments

Statistical analysis of the results was performed with Minitab (Version 19) using ANOVA. RSM based on BBD was utilized to investigate the influence of time (A), concentration (B), salinity (C) and pH (D) on the adsorption capacity of reservoir fines by MSNP. Supplementary data, Table S1 shows the levels, ranges of the independent variables and their codes. The coding of the variables was done using Equation (7).

$$X_i = \frac{(x_i - x_0)}{\Delta x_i} \tag{7}$$

whereas X_i is coded ith variable, x_i is actual ith variable, x_0 is centre point values for ith variable and Δx_i is change in step of x variable. The centre point was replicated three times to evaluate errors. Statistical analysis was used to reduce the number of experimental runs to 28 and all the coefficient of quadratic regression model and interaction factors were determined using a second order polynomial model (Equation (8)).

$$Y = b_0 + \sum_{i=1}^{n} b_i x_i + \sum_{i=1}^{n} b_{ii} x_i^2 + \sum_{i=1}^{n-1} \sum_{j=2}^{n} b_{ij} x_i x_j + \varepsilon \tag{8}$$

whereas Y is response, b_0 is intercept, b_i, b_{ii} and b_{ij} are coefficients, x_i and x_j are independent variables and ε is error.

3. Results and discussion

3.1. Thermally treated EFBA

The chemical composition of the EFBA before and after treatment was determined by XRF (Table S2). The EFBA before treatment showed 60% SiO_2 and trace-elements such as MgO, Al_2O_3, phosphorus pentoxide (P_2O_5), potassium oxide (K_2O), calcium oxide (CaO), titanium oxide (TiO_2), and iron (iii) oxide (Fe_2O_3). The thermal treatment improved the SiO_2 content to serve as alternative source of SiO_2. The XRF results (Table S2) show a significant reduction in the concentration of the trace element with increase in temperature and a corresponding increase in SiO_2 content. This is because as the temperature exceed the phase transition temperature (573 °C), the SiO_2 become loose and the high temperature causes the trace element to be active [24,25]. Consequently, some of the trace

element diffused into the surrounding SiO_2-matrix leaving a more SiO_2 rich phase, which concurs with prior findings by Fernandes et al. [16] and Shihab and Twej, [26]. They explained that thermal treatment of rice husk ash increased the SiO_2 content up to 98.8% and 98.02%, respectively. Hence, the higher the temperature the higher the rate of diffusion. However, diffusion is accelerated during the phase transition under thermodynamic forces.

3.2. Characterization analysis of MSNP and reservoir fines

3.2.1. Morphology result

The SEM image of untreated EFBA (Figure S2a) shows spherical, angular and irregular shapes. The treated EFBA showed a decrease in spherical shape with temperature (Figure S2b), which can be attributed to the collapse of some micro and mesopores at high temperature [27]. The particle size also increased with temperature (Figure S2b). At high temperature, crystal growth was enhanced, which promoted the emergence of a more compact structure. The result agrees with previous study by Fernandes et al. [16] who found that high temperature decreases the specific surface area values and thus increases the diameter of the particles. TEM was used to confirm the shape and size of MSNP (Fig. 1). The size of MSNP ranges from $17.78 - 46.69$ nm. The larger particles have a platy and irregular shape, while the smaller particles have a spherical shape. The irregular shape could be due to cavitation during wet milling. Subsequently, ultrasonic treatment of MSNP changed the shape of the particles from irregular and angular to spherical [28]. This confirms that the thermal treatment did not change the size and shape of the MSNP, but rather increased the surface stability [29]. Furthermore, mechanical energy of mill (collision of mill ball) imparts stress to the particles resulting to nucleation. High revolution of the ball mill (500 rpm) increased inter-particle or particle–wall collision and increased energy transfer to the particles resulting in coalescence. Also, the revolution of the ball mill might have increased the temperature thereby, squeezing the inner liquid and air from the interior to form a liquid film at the surface. This process
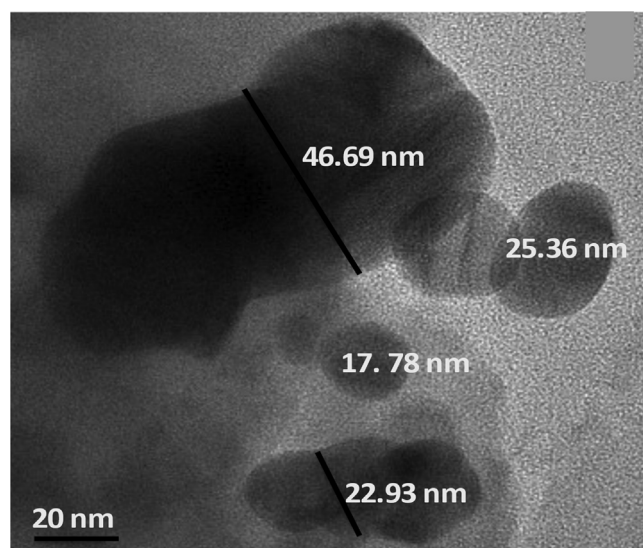
accelerates size enlargement and growth of the particles [30]. Hence, after the wet milling it was assumed that some of the MSNP resided in the aggregates with size range 22.93 nm – 46.69 nm. Hence, ultrasonication was used to disassociate the MSNP in clustered aggregates to form radicals which might have induced degradation/detexturation and sono-erosion of the MSNP reducing the size to 17.78 nm and altering the shape. FESEM image was used to visualize the adsorption of reservoir fines by MSNP. Figure S3a-b depicts the fresh images of the reservoir fines. The kaolinite surface (Figure S3a) shows a booklet shape in the form of a heterogenous layered sheets. Figure S3b indicates that the morphology of illite is fibrous. The presence of cornflakes textures indicates the presence of smectite. The FESEM images (Figure S3c-d) shows the adsorption process obtained by the static adsorption experiment. Adsorption of MSNP onto the reservoir fines had a well spread distribution signifying a monolayer coverage.

3.2.2. Surface area and porosity

The porosity of the samples was determined by nitrogen adsorption–desorption analysis. Fig. 2 shows the nitrogen adsorption of MSNP and reservoir fines. All the isotherm showed a substantial nitrogen uptake at p/p_0 higher than 0.99. The isotherm exhibits a typical type III indicating no rapid initial intake of nitrogen gas, which signifies that the forces of adsorption in the first monolayer are relatively small [31]. The absence of hysteresis loop between the adsorption–desorption indicates the presence of macroporous materials [32]. The BJH analysis of MSNP (shown as inset in Fig. 2a) indicates that the pore size distribution ranges from 2.88 to 44.8 nm suggesting a mesoporous pore structure. The broad distribution indicates that hierarchical pores appeared in the final product, which could be attributed to pore coalescence during ultrasonication [33]. The high BET surface area of MSNP (Table 1) indicated that organic matter has been broken during the thermal decomposition of EFBA resulting in a highly porous structure. Consequently, enabling adsorption of reservoir fines by MSNP thus increasing the pores size distribution (insets Fig. 2b and c). Based on the BJH results, Fig. 2b and c (insert) show a mesoporous material along with some distribution of pores above 50 nm, which suggests presence of macroporous materials in the structure. This shows the coexistence of mesoporous and macroporous materials in the structure signifying the adsorption of the reservoir fines by MSNP. This large pore size distribution might have resulted from the adsorption of the reservoir fines by MSNP [34,35]. Some micropores were also detected (Table 1), which might have developed within the MSNP by oxidation [34]. Likewise, the micropores, mesopores and total pore volume increased after adsorption of the reservoir fines by MSNP (Table 1). Indicating that some micropores are connected thereby leading to increase of mesopore volume [35].

3.2.3. Functional group analysis

The functional group and chemical compound of MSNP was determined by FTIR (Fig. 3). The band at 650–1368 cm^{-1} is a standard feature of SiO_2. The peak at 776 cm^{-1} is attributed to the symmetric of siloxane group (-Si-O-Si). The peak at 1032.31 cm^{-1} belongs to the asymmetric stretching vibrational bonds (Si-OH), which are the main peaks of SiO_2. The peak at 1742.32 cm^{-1} was due to O-H bond bending vibration from Si-

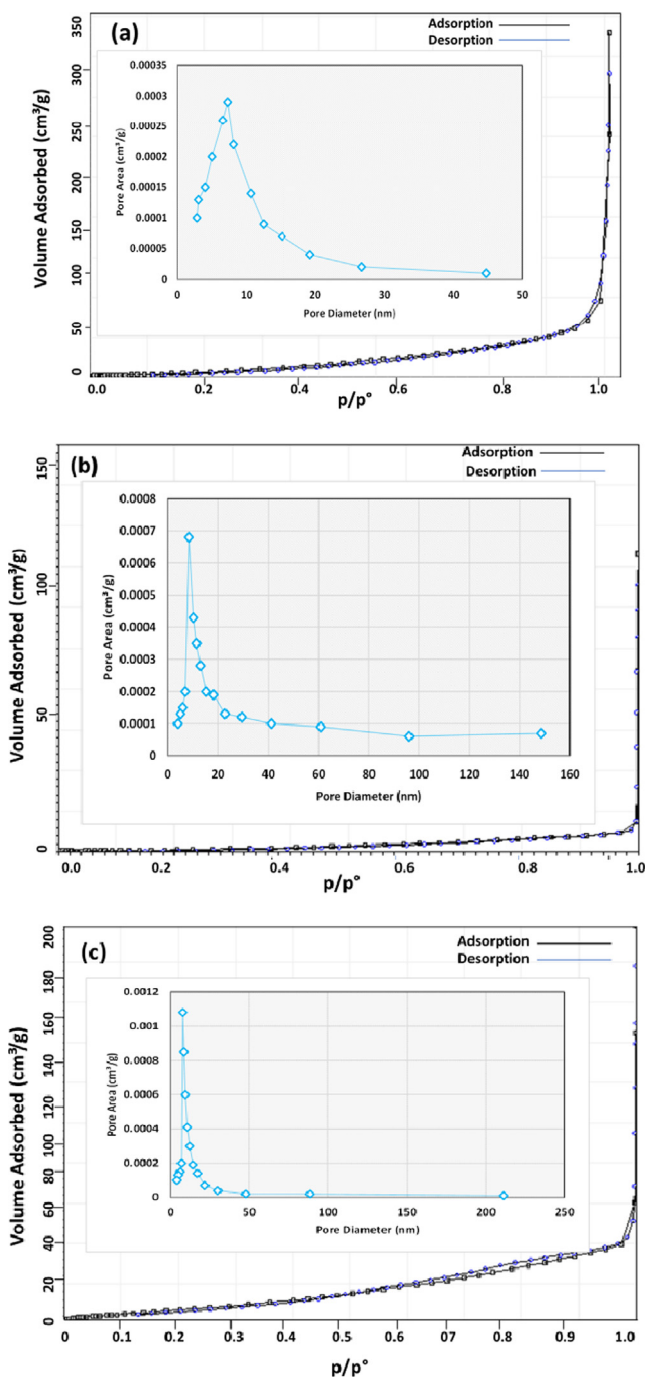**Fig. 1** TEM image of MSNP showing sizes and shape.

Fig. 2 Nitrogen adsorption–desorption isotherm (a) MSNP (b) MSNP + kaolinite (c) MSNP + illite. Inserts: corresponding pore size distribution using BJH method.

OH silanol groups [36]. The small peak occurring at 3749 cm^{-1} is assigned to the sequence in the silanol group (–OH) and hydrogen bonding of water to SiO_2 [37]. The non-appearance of any other adsorption band indicates that it is pure SiO_2. Consequently, the position of the characteristic peaks is consistent which means that the synthesis method did not change the chemical composition. The adsorption of kaolinite on MSNP showed characteristics band at 3683.9 cm^{-1} and 3619.58 cm^{-1} (Fig. 3). The band at 3619.58 cm^{-1} is ascribed

to the inner hydroxyls while the band at 3683.9 cm^{-1} is ascribed to the external hydroxyls. Subsequently, the peaks at 1113.49 cm^{-1} and 1023.64 cm^{-1} belongs to the Si-O stretching and quartz interference on the kaolinite [38]. The peaks at 995.69–910.33 cm^{-1} correspond to Al-OH bending vibration of kaolinite. The doublet at 789.98–750.46 cm^{-1} is due to Si-O-Si inter tetrahedral bridging bonds in MSNP [38]. For illite, the bands at 3696.18 cm^{-1} and 3620.45 cm^{-1} belong to hydroxyl groups bounded to illite crystals and adsorbed water, respectively. The peak at 1413.40 cm^{-1} may be due to ammonium (NH_4^+) ions. The peaks at 1002.88 cm^{-1} and 874.12 cm^{-1} are main peaks of SiO_2 from MSNP.

3.2.4. XRD analysis

The XRD results of MSNP show the presence of amorphous and crystalline phases (Fig. 4). Quartz was identified as the major crystalline phase with at sharp peak of 2θ at 26.57 ° and at 20.8 °, 50.08 ° and 59.8 °. These peaks correspond to the reflection from 011, 110, 112 and 121. Also, tridymite crystalline phase of 2θ at 21.8 °, 28.3 °, 31.1° and 36.4° corresponds to 101, 111, 102 and 200 crystal planes of alpha-SiO_2. These results matched with the standard given in the international centre of diffraction data (ICDD) 01–077-1060. This implies that the crystal plane of the SiO_2 is hexagonal with a lattice parameter of a-axis (4.9 Å), b-axis (4.9 Å) and c-axis (5.4 Å). This indicates that the MSNP has both quartz and tridymite peaks. Thermal treatment influenced the crystalline phase of the MSNP (Fig. 4). This is because high temperature supports the formation of crystalline phase due to the energy supplied to the system [16]. Hence, quartz crystallization took place between 573 and 1055 °C, whereas tridymite at 867 °C [16,39]. This might be because of diffusion induced mechanism during the wet milling might have influenced the kinetic transformation to a more crystalline phase [30]. Also, ultrasonic treatment might have decomposed the molecular chains of the MSNP by shearing, exposing the hydroxyl group. Which enhanced the interaction between the MSNP and alcohol molecules leading to destruction of the molecules in solution and recrystallization of the MSNP [40]. Nevertheless, residual amorphous phase still exists after temperature treatment [41]. Fig. 4 shows XRD results of reservoir fines. The kaolinite sample had major peaks of 2θ at 11.16° and 24.88°. The peak at 11.16° shows the presence of halloysite [42]. Minor traces of quartz were identified at 21.02° and 26.61°. The presence of quartz was identified at 26.59°. Illite showed a diffraction of 2θ at 8.82° and quartz was identified at 26.61°.

### 3.3. Effect of contact time on adsorption capacity

The adsorption rate of reservoir fines by MSNP at different concentrations is shown in Fig. 5. Adsorption rate was rapid at the beginning and slowed down with time until equilibrium was attained. This is because of the high number of MSNP active site and sufficient surface available for adsorption. Afterwards, active sites gradually saturated and lack of access to the active site, which might have instigated repulsion of unattached fines in solution. Thus, reducing the energy resulting to desorption of the MSNP at which equilibrium adsorption was attained [43,44]. Increase in concentration increased the time and ability to attain equilibrium (Fig. 5). This is because the quantity of reservoir fines active site was less than

Table 1 Summarized physicochemical properties of MSNP and reservoir fines.

Sample	BET Surface area (m^2/g)	Average Pore Diameter (nm)	Mesopore Volume (cm^3/g)	Micropore Volume (cm^3/g)	Total Pore Volume (cm^3/g)
MSNP	332	2.1	0.206	0.002	0.208
MSNP + Kaolinite	9	4.3	0.28	0.015	0.295
MSNP + Illite	120	3.9	0.24	0.006	0.246
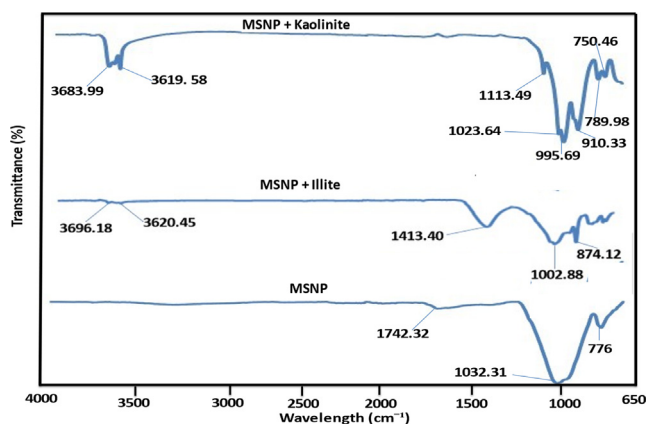
Fig. 3 FTIR spectra of MSNP before and after adsorption with reservoir fines.
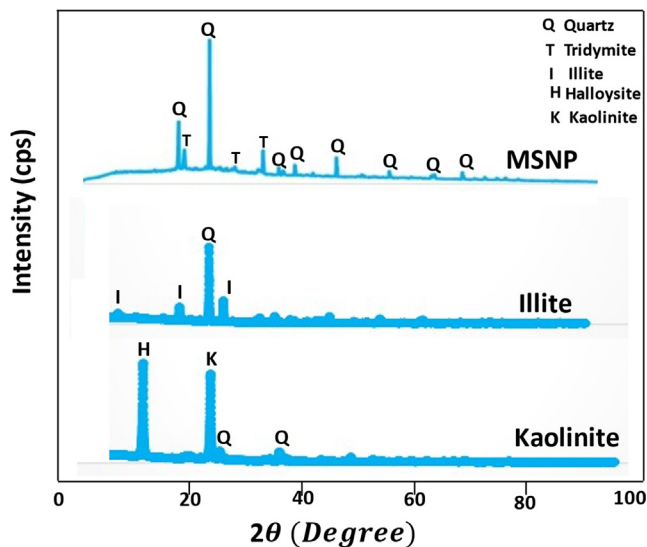
Fig. 4 XRD spectra for MSNP and reservoir fines.

that of MSNP thereby, shortening interaction duration. However, at high concentration more fines are in solution and a larger energy is needed to overwhelm the resistance for adsorption. Hence, more time might be required for the fines to adhere onto the MSNP [44,45]. For illite at low concentration (10 mg/L and 15 mg/L), the diffusion of the molecules to the adsorption site of the MSNP required more time initially whereas at higher concentration (20 mg/L and 25 mg/L), the migration of the molecules from the solution to MSNP was rapid [13,44]. During the migration process the ions of the illite
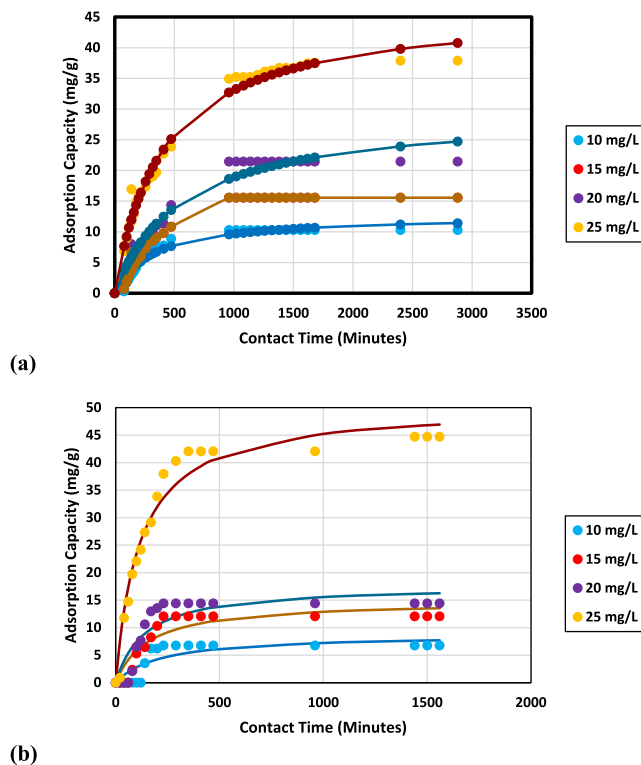
Fig. 5 Reservoir fines adsorption by MSNP (a) kaolinite and (b) illite (lines were predicted using pseudo-second order).

might have been temporarily adsorbed by the adsorption site on the wall of the MSNP thereby delaying the adsorption by reducing the effective cross-section of the pores and hindering the migration of other ions [31].

3.4. Adsorption kinetics model

Pseudo-first and second order adsorption models were used to analyse reservoir fines adsorption rate by MSNP. Pseudo first order assumes that reservoir fines adsorption rate intensification is proportionately to the number of fines adsorbed. Hence, the process is governed by availability of adsorption sites. Table 2 summarises reservoir fines kinetic adsorption by MSNP. Results indicate that the adsorption of reservoir fines onto MSNP did not fit into the first order model because of inconsistent adsorption profile as a result of intrinsic microporosity restricting MSNP molecule's diffusion to the pore channel of the reservoir fines [45]. Contrarily, for illite at higher concentration of 25 mg/L the regression coefficient (R^2) of 0.98 shows a fit to the pseudo-first order. This signifies

that more than one mechanism has contributed to the adsorption process which is consistent with the adsorption rate of illite at different concentration (Fig. 5b). The pseudo-second order having R^2 of 0.99 shows that the model best describe reservoir fines adsorption rate by MSNP at the concentration investigated. This signifies that the adsorption process was governed by chemical adsorption through interchange or splitting of electrons between reservoir fines and MSNP [46]. Pseudo-second order rate constant (K_2) decreased as concentration of reservoir fines increased. At low concentration there is a weak activation energy due to less repulsion of reservoir fines molecules resulting in a high-rate constant. However, at higher concentration, the collision of reservoir fines intensifies, decreasing the rate constant [45]. Initial adsorption rate (h) increased with increase in concentration of reservoir fines, which might be because of the characteristics of the reservoir fines. Similar result was observed by previous studies of Tan and Zaini [44] and Hameed et al. [47] when they stated that the physicochemical characteristics of adsorbent and adsorbate can influence the h values.

3.5. Effect of concentration on adsorption of reservoir fines by MSNP

Adsorption of reservoir fines at different concentrations onto MSNP is depicted in Fig. 6. An increasing trend of adsorption as the concentration increases was observed until equilibrium was attained. At equilibrium, the quantity of reservoir fines desorbed is equal to the quantity adsorbed. At low concentration, the adsorption capacity was low. This is because initial concentration energy of the solute reduced the mass transfer resistance of the reservoir fines. Subsequently, reservoir fines adsorption improved with increased concentration gradient and initial concentration [48]. This implies that the equilibrium adsorption capacity is concentration dependent [49].

3.6. Adsorption isotherm model

Adsorption isotherms explains how adsorption molecules interacts when the adsorption process reaches equilibrium state. Langmuir and Freundlich models were used to describe the equilibrium correlation at different initial concentration (Table 3). Table 3 depicts that the equilibrium data of reservoir fines adsorption by MSNP followed Langmuir model. Hence, the adsorption could be described as single-layered coverage of MSNP on a homogenous surface, which is consistent with the kinetic adsorption studies of chemosorption. The validity of Langmuir model on the adsorption was determined by a separation factor:

$$R_L = \frac{1}{1 + K_L C_o} \qquad (9)$$

whereas R_L is equilibrium parameter. It was utilized in determining the viability of reservoir fines adsorption by MSNP. Hence, $R_L > 1$ is unfavourable, $R_L = 1$ is linear, $0 < R_L < 1$ is favourable and $R_L = 0$ is irreversible. Table 3 indicates that R_L was < 1 signifying a favourable adsorption and strong bonding. This indicates that the active sites undergoing adsorption occurred at specific sites until a monolayer was formed. Also, the value of Langmuir constant (K_L) between 0.6 and 0.63 shows a favourable adsorption of the

Table 2 Pseudo-kinetics constants of reservoir fines adsorption on MSNP.

Pseudo-first Order

	10 mg/L K	10 mg/L I	15 mg/L K	15 mg/L I	20 mg/L K	20 mg/L I	25 mg/L K	25 mg/L I
Exp q_e (mg/g)	10	7	16	12	21	14	38	45
q_e (mg/g)	8	4.	11	8	15	10	26	45
K_1 (h^{-1})	1	1	1	1	1	1	1	0.006
R^2	0.2	0.09	0.12	0.14	0.11	0.14	0.15	0.98
SSE	299	173	803	387	1610	577	3552	47

Pseudo-second Order

	10 mg/L K	10 mg/L I	15 mg/L K	15 mg/L I	20 mg/L K	20 mg/L I	25 mg/L K	25 mg/L I
Exp q_e (mg/g)	10	7	16	12	21	14	38	45
q_e (mg/g)	13	9	21	15	30	18	47	50
K_2 (g/mg h)	0.0002	0.0005	0.0001	0.0004	6E-05	0.0004	5E-05	0.0001
h (mg/g h)	0.04	0.04	0.04	0.09	0.05	0.12	0.1	0.43
R^2	0.94	0.74	0.96	0.86	0.97	0.83	0.99	0.97
SSE	21	52	34	69	60	125	62	146

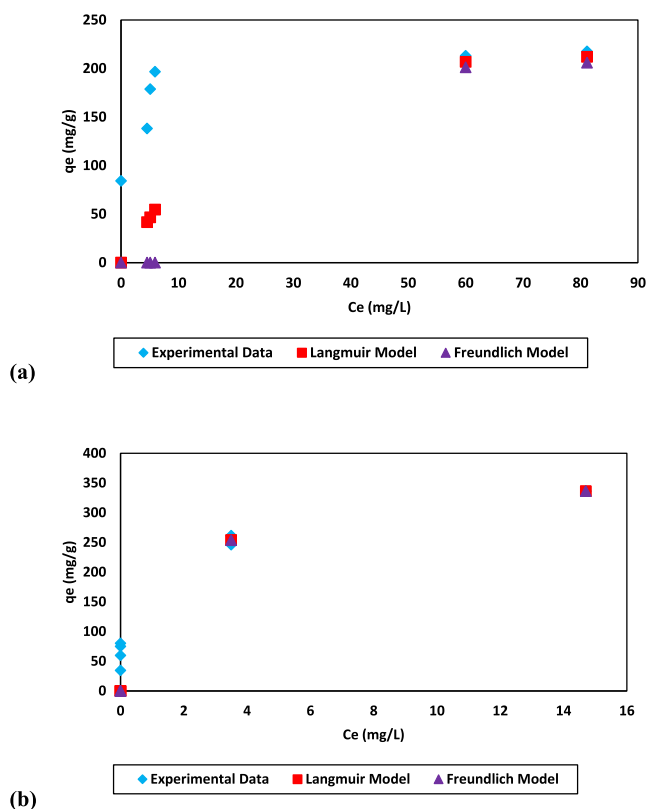*K: Kaolinite and I: Illite.

(a)

(b)

Fig. 6 Experimental equilibrium adsorption of reservoir fines by MSNP fitted to Langmuir and Freundlich models (a) kaolinite and (b) illite.

reservoir fines by MSNP [50]. The fitting to Freundlich model showed low regression values for kaolinite suggesting a single layer coverage. Whereas Freundlich model gave a good fit for illite indicating that it is not limited to only monolayer coverage or any uniform distribution [32]. The value of n between 5 and 11 shows sufficient site for adsorption [46]. Comparing the R^2 of both models, it can be concluded that the adsorption isotherm data of kaolinite reservoir fines adsorption by MSNP can be described by Langmuir model rather than Freundlich. However, considering the high R^2 value and lower SSE value of illite for Freundlich model indicates the pertinence of this model is better than Langmuir model [51,52]. Also, the value of $1/n < 1$ indicates that the adsorption process is chemosorption [53].

3.7. Effect of salinity on adsorption capacity

The impact of electrolyte on reservoir fines adsorption by MSNP is illustrated by the plot of equilibrium adsorption as a function of salinity concentration (Fig. 7). Increase in concentration of electrolyte resulted in higher adsorption. The increase might be because of the increased amount of positively charged (Na +) cation on reservoir fines which increased the electrostatic contact between MSNP's negatively charged oxygen and positively charged (Na^+) cation of NaCl [54]. Likewise, Na^+ can form bridges of cation between the negatively charged MSNP and negatively charged reservoir fines layers. Consequently, the cation bridges formed between the MSNP molecules compressed it further thereby, more MSNP were adsorbed. This signifies that electrolyte can affect surface charge and alter the level of electrostatic interactions [13]. Also, the neutralizing bridges between MSNP and negative charge of reservoir fines led to indirect adsorption.

3.8. Effect of pH on adsorption capacity

Initial pH of solution can control the adsorption capacity by altering the surface charge and functional group on the surface of the MSNP. Fig. 8 shows the effect of pH on reservoir fines adsorption by MSNP. Adsorption capacity increased at low pH from 2 to 4, with the further increase in pH from 6 to 10, the adsorption capacity decreased. This is due to protonation of the active sites on the surface of MSNP at pH less than point of zero charge (pHpzc), which enhanced the positive charge on its surface. Thus, the adsorption capacity was enhanced as result of strong electrostatic interaction between the MSNP and reservoir fines. As the pH increases above the pHpcz of MSNP (4.2), the negative sites from the silanol group on the SiO_2 surface improves according to the following reaction.

$$-SiOH + OH^- \leftrightharpoons -SiO^- + H_2O \qquad (10)$$
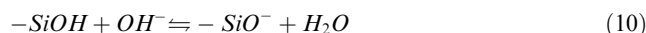
Hence, the surface of the MSNP becomes more negative at higher pH and Al-O and Si-O faces on the reservoir fines surface carries a negative charge at higher pH [55], electrostatic repulsion prevails decreasing adsorption capacity.

3.9. MSNP reusability

The reusability test was carried out on the MSNP to determine the number of times it can be reused before the adsorption capability reach below 50%. Figure S4 shows the adsorption efficiency of MSNP on reservoir fines. MSNP retained

Table 3 Isotherm constants for reservoir fines adsorption by MSNP.

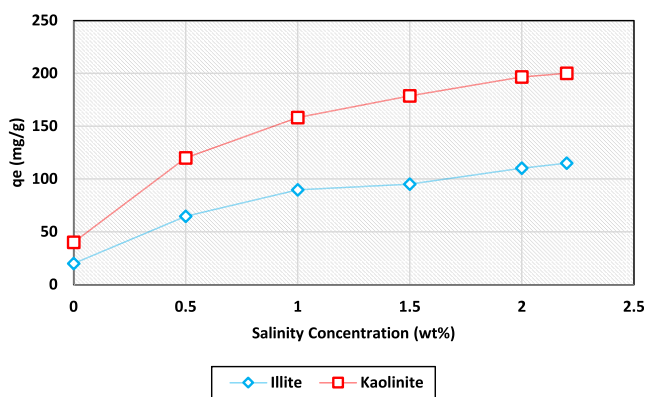| Isotherm Model	Langmuir			Freundlich	
Reservoir Fines	Kaolinite	Illite		Kaolinite	Illite
Expq_e (mg/g)	218	336	Expq_e (mg/g)	218	336
q_m (mg/g)	223	374	K_F(mg/g) (L/mg)$^{1/n}$	147	199
K_L (L/mg)	0.63	0.6	$1/n$	0.0913	0.195
R^2	0.86	0.985	R^2	0.62	0.98
R_L	0.002	0.0016	n	11	5
SSE	8343	16,976	SSE	1569	121

Fig. 7 Impact of electrolyte on the adsorption of MSNP on reservoir fines.
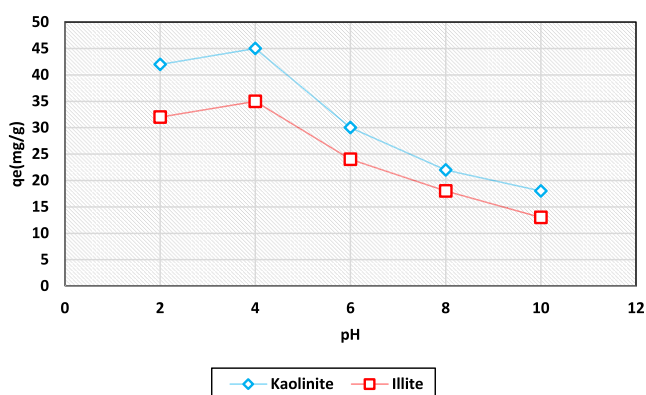

Fig. 8 Effect of initial pH on adsorption of reservoir fines by MSNP.

80–90% of its adsorption efficiency up to the 5th cycle. This could be attributed to the stability of the active sites of the MSNP. The activity of the MSNP declined below 50% in the 6th cycle. This might be because of leaching of the active sites due to repeated washing which could have reduced the efficacy of the MSNP [14,56]. This implies that MSNP is relatively stable up to five consecutive cycles.

3.10. Statistical analysis of the adsorption process

The empirical model's equation between the adsorption capacity and input factors in coded term are given as Equation 11–12.

$$
\begin{aligned}
AdsorptionCapacity(K) = & -83.5 + 0.0013A + 0.3269B \\
& + 169.7C + 1.08D \\
& - 0.000001A * A \\
& - 0.000207B * B - 33.7C * C \\
& - 0.072D * D + 0.00000A * B \\
& + 0.00008A * C - 0.000000A \\
& * D + 0.0361B * C \\
& - 0.01060B * D - 5.64C * D
\end{aligned} \quad (11)
$$

$$
\begin{aligned}
AdsorptionCapacity(I) = & -346 + 0.0044A + 1.212B \\
& + 370C + 25.3D - 0.000003A \\
& * A - 0.000565B * B - 61.1C \\
& * C - 0.332D * D \\
& + 0.000000A * B - 0.0000A \\
& * C + 0.00000A * D + 0.2440B \\
& * C - 0.06782B * D - 21.94C * D
\end{aligned} \quad (12)
$$

whereas K and I are kaolinite and illite, respectively. The positive values in Equations 11–12 signifies that the parameter has a positive and direct correlation with the reservoir fines adsorption. The negative sign shows an inverse relation between the response and the parameter. ANOVA analysis was used to evaluate the quality and importance of the designed model (Table S3). The degree of freedom (DF), adjusted sum of square (SS), adjusted mean square (MS), Fisher (F)-value, probability (P)-value and the contributions of each parameter in the model prediction are presented in the ANOVA tables (Table S3). The F and P-values (Tables S3) signifies that concentration, salinity and pH are the main parameters whereas time is insignificant. Also, the model terms are deemed significant when $p < 0.05$ [57] hence, B, C, D, B*B, B*C, B*D, C*C (illite) and C*D are significant model terms. The terms A, A*A, C*C (kaolinite), D*D, A*B, A*C, A*D are insignificant. Therefore, for better predictability the insignificant terms determined by ANOVA were expunged from Equations (11) and (12). The revised quadratic equation in coded terms are:

$$
\begin{aligned}
AdsorptionCapacity(K) = & -83.5 + 0.3269B + 169.7C \\
& + 1.08D - 0.000207B * B \\
& + 0.0361B * C - 0.01060B \\
& * D - 5.64C * D
\end{aligned} \quad (13)
$$

$$
\begin{aligned}
AdsorptionCapacity(I) = & -346 + 1.212B + 370C \\
& + 25.3D - 0.000565B * B \\
& - 61.1C * C + 0.2440B * C \\
& - 0.06782B * D
\end{aligned} \quad (14)
$$

Table S4 shows the coefficient of determination (R^2), R^2 adjusted and R^2 predicted. Kaolinite with R^2 value of 98.77% and illite (99.32%) close to unity indicates that the model is highly consistent with the experimental results for the reservoir fines with high precision and reliability. This shows relationship between the experimental values and that predicted by the model. Therefore, it can be used to predict the response at any level of the selected factor with high accuracy. The plot of the normal probability versus residuals of the model (Figure S5) reveals no significant scattering of the experimental data, proving the model's precision. Figure S6 shows the degree to which the residual and projected values are similar. The order of observation versus the residual responses (Figure S7) shows all the residual random scatter were consistently distributed along the run number indicating that there is a strong link between the experimental and expected responses. This confirms the independence of each experiment. Figure S8

shows that majority of the values falls along the origin and the scatter values were minimal. Finally, the Pareto chart for the standardized effect of the various factors on reservoir fines adsorption by MSNP (Figure S9) indicates that at a confidence level of 95%, pH is the most significant factor, followed by concentration and salinity.

3.11. Effect of interaction variables on the efficacy of reservoir fines adsorption

The interaction between factors and responses was examined using a three-dimensional (3D) response surface plot (Figure S10). The surface plots show the function of two factors while keeping the other two factors fixed. Figure S10a-b shows the interaction between initial concentration and time. The simultaneous increase in concentration and time increased the adsorption capacity of the MSNP. But at low concentration and prolonged time, the adsorption capacity did not increase. This implies that the increase in concentration was responsible for the increased adsorption capacity. The effect of pH was investigated against salinity (Figure S10 c-d). It was observed that at low pH and high salinity the adsorption capacity increased. Also, at high pH and low salinity the adsorption capacity was still significant. This implies that both pH and salinity influenced the adsorption capacity.

3.12. Optimization study

The optimum of the process parameters to maximize the adsorption capacity of reservoir fines by MSNP from the mathematical model equations developed from this study was investigated. A multiple response method was applied to optimize any combination of the variables at which the maximum adsorption of the reservoir fines occurred. All the parameters were set to be in range while the adsorption capacity was set to maximize. Figure S11 shows the desirability graph generated from the optimal points through the numerical optimization. The maximum adsorption capacity for kaolinite was obtained at time 1591 min, initial concentration of 932.8 mg/g, salinity of 2.2 wt% and pH 2. Whereas the maximum adsorption capacity for illite was at time 737 min, initial concentration of 1000 mg/g, salinity of 2.2 wt% and pH 2 (Figure S11). The desirability of 1.00 signifies that the process has the acceptable adsorption capacity at the operating condition.

4. Limitation and recommendation

The present work was carried out at ambient condition which does not depict the ideal reservoir conditions. Hence, the influence of temperature on the adsorption capacity needs to be investigated. Also, the static adsorption needs to be correlated with the dynamic adsorption studies in the presence of crude oil. Previous studies on dynamic adsorption are mainly on sandpacks and glass beads porous media. The use of these porous media is only symbolic it does consider the heterogeneity of a reservoir. Moreso, during the dynamic displacement process using sandpack and glass beads the movement of fluid through the side wall of these porous media is often ignored. Hence, the use of reservoir cores to simulate reservoir conditions (oil, salinity, pressure and temperature) is highly recommended.

5. Conclusions

The combined methods of wet milling and ultrasonication was utilized to produce MSNP to trap reservoir fines at static condition. The experimental results show that pseudo-second order model best describe the adsorption process. Langmuir isotherm model best fitted the equilibrium adsorption of kaolinite by MSNP compared to the Freundlich model. However, the equilibrium adsorption of illite by MSNP best fitted the Freundlich model. The predicted reservoir fines adsorption close to unity indicates that the model is highly consistent with the experimental results with high precision and reliability. Statistical and parametric analysis indicated that the optimum values for achieving the maximum adsorption capacity were pH 2, salinity 2.2 wt%, time 1591 min and 737 min, initial concentration of 932.8 mg/g and 1000 mg/g for kaolinite and illite, respectively. Experimental results have shown that MSNP can fixate reservoir fines at static condition and has adequate capacity to be rejuvenated and reused.

Declaration of Competing Interest

The authors declare that they have no known competing financial interests or personal relationships that could have appeared to influence the work reported in this paper.

Acknowledgement

Appendix A. Supplementary material

Supplementary data to this article can be found online at https://doi.org/10.1016/j.aej.2022.02.016.

References

[1] A. Agi, R. Junin, M.O. Abdullah, M.Z. Jaafar, A. Arsad, W.R. Wan Sulaiman, M.N.A. Norddin, M. Abdurrahman, A. Abbas, A. Gbadamosi, N.B. Azli, Application of polymeric nanofluid in enhancing oil recovery at reservoir condition, J. Pet. Sci. and Eng. 194 (2020) 107476.

[2] A. Agi, R. Junin, M.Z. Jaafar, M.A. Sidek, F. Yakasai, A. Gbadamosi, J. Oseh, Formulation of Bionanomaterials: A Review of Particle Design Towards Oil Recovery Applications, J. Ind. and Eng. Che. 98 (2021) 82–102.

[3] F. Yakasai, M.Z. Jaafar, S. Bandyopadhyay, A. Agi, Current developments and future outlook in nanofluid flooding: A comprehensive review of various parameters influencing oil recovery mechanisms, J. Ind. Eng. Che. 93 (2021) 138–162.

[4] X. Zhao, Z. Qiu, J. Gao, X. Ren, J. Li, W. Huang, Mechanism and Effect of Nanoparticles on Controlling Fines Migration in Unconsolidated Sandstone Formations, SPE J. 26 (06) (2021) 3819–3831, https://doi.org/10.2118/204474-PA.

[5] K. Prempeh, L. Chequer, A. Badalyan, P. Bedrikovetsky, Effects of the capillary-entrapped phase on fines migration in porous media, J. Nat. Gas Sci. Eng. 73 (2020) 103047.

[6] B. Yuan, R. Moghanloo, P. Pattamasigh, Applying Method of Characteristics to Study Utilization of Nanoparticles to Reduce Fines Migration in Deepwater Reservoirs. Paper SPE- -174192-

MS, presentation at the SPE European Formation Damage Conference and Exhibition held in Budapest, Hungary, 3–5 June (2015).

[7] L. Giraldo, R. Diez, S. Acevedo, F. Cortes, C. Franco, The effects of chemical composition of fines and nanoparticles on inhibition of formation damage caused by fines migration: Insights through a simplex-centroid mixture design of experiments, J. Pet. Sci and Eng. 203 (2021) 108494.

[8] N. Ogolo, E. Iloke, G. Godstime, M. Onyekonwu, Mobilization of Clayey Fines by Different Water Salinity Values in the Presence of Aluminium Oxide Nanoparticles, Paper SPE-189125-MS presented at the Nigerian Annual Conference and Exhibition held in Lagos, 2017.

[9] M. Mansouri, A. Nakhaee, P. Pourafshary, Effect of SiO_2 nanoparticles on fines stabilization during low salinity water flooding in sandstones, J. Pet. Sci. and Eng. 174 (2019) 637–648.

[10] R. Diez, O. Medina, L. Giraldo, F. Cortes, C. Franco, Development of Nanofluids for the Inhibition of Formation Damage Caused by Fines Migration: Effect of the Interaction of Quaternary Amine (CTAB) and MgO Nanoparticles, Nanomaterials 10 (2020) 928.

[11] M. Mansour, M. Eleraki, A. Noah, E.-A. Moustafa, Using nanotechnology to prevent fines migration while production, Petroleum 7 (2) (2021) 168–177.

[12] S. Shafian, I. Saaid, N. Razali, I. Salleh, S. Irawan, Experimental investigation of colloidal silica nanoparticles (C-SNPs) for fines migration control application, App. Nanosci. 11 (2021) 1993–2008.

[13] A. Monfared, M. Ghazanfari, M. Jamialahmadi, A. Helalizadeh, Adsorption of Silica Nanoparticles onto Calcite: Equilibrium, Kinetics, Thermodynamics and DLVO Analysis, Che. Eng. J. 281 (2015) 334–344.

[14] R.V. Quah, Y.H. Tan, N.M. Mubarak, J. Kansedo, M. Khalid, E.C. Abdullah, M.O. Abdullah, Magnetic biochar derived from waste palm kernel shell for biodiesel production via sulfonation, Waste Manag. 118 (2020) 626–636.

[15] T.G. Pineda-Vásquez, A.E. Casas-Botero, M.E. Ramírez-Carmona, M.M. Torres-Taborda, C.H.L. Soares, D. Hotza, Biogeneration of Silica Nanoparticles from Rice Husk Ash Using Fusarium oxysporum in Two Different Growth Media, Ind. Eng. Chem. Res. 53 (17) (2014) 6959–6965.

[16] I.J. Fernandes, F. Sanchez, J. Jurado, A. Kieling, T. Rocha, C. Maraes, V. Sousa, Physical, Chemical and Electrical Characterization of Thermally Treated Rice Husk Ash and Its Potential Application as a Ceramic Raw Material, Adv. Powd. Techno. 28 (2017) 1228–1236.

[17] A. Masood, S. Maheen, H. Khan, S.S. Shafqat, M. Irshad, I. Aslam, A. Rasul, S. Bashir, M. Zafar, Pharmaco-Technical Evaluation of Statistically Formulated and Optimized Dual Drug-Loaded Silica Nanoparticles for Improved Antifungal Efficacy and Wound Healing, ACS Omega 6 (2021) 8210–8225.

[18] K. Lee, Continuous granulation of pharmaceutical powder using a twin screw granulator, University of Birmingham, 2013, PhD Thesis.

[19] A. Agi, R. Junin, A. Gbadamosi, A. Abbas, N.B. Azli, J. Oseh, Influence of Nanoprecipitation on Crystalline Starch Nanoparticles formed by Ultrasonic Assisted Weak-Acid Hydrolysis of Cassava Starch and the rheology of their Solutions, Che. Eng. and Proc- Pro Inten. 142 (2019) 107556.

[20] N. Rahman, M. Nasir, Application of Box-Behnken design and desirability function in the optimization of Cd(II) removal from aqueous solution using poly(o-phenylenediamine)/hydrous zirconium oxide composite: equilibrium modeling, kinetic and thermodynamic studies, Env. Sci and Poll. Res. 25 (26) (2018) 26114–26134.

[21] N. Rahman, M. Nasir, P. Varshney, A.M. Al-Enizi, M. Ubaidullah, S.F. Shaikh, M.A. Al-Adrabalnabi, Efficient removal of Pb(II) from water using silica gel functionalized with thiosalicylic acid: Response surface methodology for optimization, J. K. S. Uni – Sci 33 (1) (2021) 101232.

[22] S.N.H. Azmi, B.M.H. Al-Jassasi, H.M.S. Al-Sawafi, S.H.G. Al-Shukaili, N. Rahman, M. Nasir, Optimization for synthesis of silver nanoparticles through response surface methodology using leaf extract of Boswellia sacra and its application in antimicrobial activity, Environ Monit Ass. 193 (2021) 497.

[23] N. Rahman, P. Varshney, Facile Synthesis and Characterization of Zn(II)-Impregnated Chitosan/Graphene Oxide: Evaluation of Its Efficiency for Removal of Ciprofoxacin from Aqueous Solution, J. of Inorg and Organo Poly. and Mat. 31 (2021) 3595–3612.

[24] Y. Jani, W. Hogland, Reduction-melting extraction of trace elements from hazardous waste glass from an old glasswork's dump in the South Eastern part of Sweden, Environ Sci Pollut Res. 24 (2017) 26341–26349.

[25] F. Li, X. Jiang, Q. Zuo, J. Li, B. Ban, J. Chen, Purification Mechanism of Quartz Sand by Combination of Microwave Heating and Ultrasound Assisted Acid Leaching Treatment. Silicon (2020)

[26] B. Shihab, W. Twej, Influence of chemical and thermal treatment on the purity of silica extracted from rice husk, Ira. J. of Phy. 16 (39) (2018) 117–123.

[27] G. Liu, B. Zhou, A. Du, A. Shen, Q. Yu, Effect of the thermal treatment on microstructure and physical properties of low-density and high transparency silica aerogels via acetonitrile supercritical drying, J Porous Mater. 20 (2013) 1163–1170.

[28] M. Ahmad, A. Gani, I. Hassan, Q. Huang, H. Shabbir, Production and characterization of starch nanoparticles by mild alkali hydrolysis and ultra-sonication process, Sci. Rep. 10 (2020) 3533.

[29] S. Reynolds, K. Markland, J. Rood, E. Leonard, S. Saunders, Manipulating Ligand-Nanoparticles Interaction and Catalytic Activity Through Organic-Aqueous Tunable Solvent Recovery, RSC Adv. 6 (2016) 78496–78504.

[30] A. Agi, R. Junin, M.Z. Jaafar, R. Mohsin, A. Arsad, A. Gbadamosi, C.K. Fung, J. Gbonhinbor, Synthesis and Application of Rice Husk Silica Nanoparticles for Chemical Enhanced Oil Recovery, J. Mat Res and Tech 9 (6) (2020) 13054–13066.

[31] Q. Chang, Surface of Solids, in: In: Colloids and Interface Chemistry for Water Quality Control, 2016, pp. 175–225.

[32] S. Rovani, J. Santos, P. Corio, D. Fungaro, Highly Pure Silica Nanoparticles with High Adsorption Capacity Obtained from Sugarcane Waste Ash, ACS Omega 3 (2018) 2618–2627.

[33] K. Chen, Z. Bao, A. Du, X. Zhu, G. Wu, J. Shen, B. Zhou, Synthesis of resorcinol–formaldehyde/silica composite aerogels and their low-temperature conversion to mesoporous silicon carbide, Micro. and Meso. Mat. 149 (2012) 16–24.

[34] H. Zhang, X. Zhao, X. Ding, H. Lei, X. Chen, D. An, Y. Li, Z. Wang, A study on the consecutive preparation of D-xylose and pure superfine silica from rice husk, Bio. Tech. 101 (2010) 1263–1267.

[35] V. Vanezia, F. Sannino, A. Costantini, B. Silvestri, S. Cimino, V. Califano, Mesoporous silica nanoparticles for β-glucosidase immobilization by templating with a green material: Tannic acid, Micro. and Meso. Mat. 302 (2020) 110203.

[36] P.E. Imoisili, K.O. Ukoba, T.-C. Jen, Green technology extraction and characterisation of silica nanoparticles from palm kernel shell ash via sol–gel, J. Mater, Res. Techno. 9 (1) (2020) 307–313.

[37] K. Tettey, D. Lee, Effect of Thermal Treatment and Moisture Content on the Charge of Silica Particles in Non-Polar Media, Soft Matter 9 (2013) 7242–7250.

[38] B.J. Siakia, G. Parthasarathy, Fourier Transform Infrared Spectroscopic Characterization of Kaolinite from Assam and Meghalaya, Northeastern India, J. Mod. Phys. 1 (2010) 206–210.

[39] M. Borouni, B. Niroumand, A. Maleki, A study on crystallization of amorphous nano silica particles by mechanical activation at the presence of pure aluminum, J. Solid-State Che. 263 (2018) 208–215.

[40] X. Lin, S. Sun, B. Wang, B. Zheng, Z. Guo, Structural and physicochemical properties of lotus seed starch nanoparticles prepared using ultrasonic-assisted enzymatic hydrolysis, Ultra Sono 68 (2020) 105199.

[41] G. Drisko, A. Carettero-Genevrier, A. Perrot, M. Gich, J. Gazquez, J. Rodriguez-Carvajal, L. Favre, D. Grosso, C. Boissière, C. Sanchez, Crystallization of hollow mesoporous silica nanoparticles, Chem. Commun. 51 (2015) 4164–4167.

[42] R. Dewi, H. Agusnar, Z. Alfian, Tarin: Characterization of technical kaolin using XRF, SEM, XRD, FTIR and its potentials as industrial raw materials. Journal of Physics: Conf. Series (2018)

[43] R. Foroutan, S. Peighambardoust, R. Mohammadi, M. Omidvar, G. Sorial, B. Ramavandi, Influence of Chitosan and Magnetic Iron Nanoparticles on Chromium Adsorption Behaviour of Natural Clay: Adaptive Neuro-fuzzy Inference Modelling, Int. J. Bio Macro. 15 (2020) 355–365.

[44] S. Tang, M. Zaini, Microporous activated carbon prepared from yarn processing sludge via composite chemical activation for excellent adsorptive removal of malachite green, Surf. and Interf. 22 (2021) 100832.

[45] A. Faizal, M. Halim, M. Zaini, Kinetics and dynamic adsorption of methylene blue by CO_2-activated resorcinol formaldehyde carbon gels, C. Lett 29 (2019) 319–326.

[46] A. Faizal, M. Zaini, Dyes adsorption properties of KOH-activated resorcinol-formaldehyde carbon gels -kinetic, isotherm and dynamic studies. T. Rev. (2020) 10.1080/15569543.2020.1857773

[47] B.H. Hameed, I.A.W. Tan, A.L. Ahmad, Adsorption isotherm, kinetic modeling and mechanism of 2,4,6-trichlorophenol on coconut husk-based activated carbon, Chem. Eng. J. 144 (2) (2008) 235–244.

[48] S. Mamah, P.S. Goh, A.F. Ismail, M. Amin, N. Ahmad, N.D. Suzaimi, Y. Raji, Facile preparation of palygorskite/chitin nanofibers hybrids nanomaterial with remarkable adsorption capacity, Mat. Sci. and Eng. B 262 (2020) 114725.

[49] N.D. Suzaimi, P.S. Goh, N. Malek, J. Lim, A.F. Ismail, Enhancing the Performance of Porous Rice Husk Silica Through Branched Polyethyleneimine Grafting for Phosphate Adsorption, Arab. J. Che 13 (2020) 6682–6695.

[50] S.S. Shafqat, A.A. Khan, M.N. Zafar, M.H. Alhaji, K. Sanaullah, S.R. Shafqat, S. Murtaza, S.C. Pang, Development of amino-functionalized silica nanoparticles for efficient and rapid removal of COD from pre-treated palm oil effluent, J. Mat. Res and Tech. 8 (1) (2019) 385–395.

[51] N. Rahman, U. Haseen, Equilibrium Modeling, Kinetic, and Thermodynamic Studies on Adsorption of Pb(II) by a Hybrid Inorganic−Organic Material: Polyacrylamide Zirconium(IV) Iodate, Ind. Eng. Chem. Res. 53 (19) (2014) 8198–8207.

[52] N. Rahman, P. Varshney, Assessment of ampicillin removal efficiency from aqueous solution by polydopamine/zirconium (iv) iodate: optimization by response surface methodology, RSC Adv. 10 (2020) 20322–20337.

[53] N. Rahman, M.F. Khan, M. Nasir, Experimental design approach for optimization of Pb(II) removal from aqueous solution using poly-o-toluidine/stannic(IV) triethanolamine as adsorbent, Env Techn & Inno 17 (2020) 100634.

[54] M.S. Musa, W. Sulaiman, Z. Majid, Z. Majid, A. Idris, K. Rajaei, Henna extract as a potential sacrificial agent in reducing surfactant adsorption on kaolinite: The role of salinity. J. K S Uni. –, Eng. Sci 32 (2020) 543–547.

[55] X. Lu, T. Lu, H. Zhang, Z. Shang, J. Chen, Y. Wang, D. Li, Y. Zhou, Z. Qi, Effects of solution chemistry on the attachment of graphene oxide onto clay minerals, Environ. Sci. Proc Imp. 21 (2019) 506–513.

[56] E. Onoja, S. Chandren, F. Ilyana, A. Razak, R. Wahab, Extraction of nanosilica from oil palm leaves and its application as support for lipase immobilization, J. Biotech. 283 (2018) 81–96.

[57] N. Rahman, M. Nasir, Effective removal of acetaminophen from aqueous solution using Ca (II)-doped chitosan/β-cyclodextrin composite, J. Mol. Liq 301 (2020) 112454.